Hindawi Publishing Corporation
Laser Chemistry
Volume 2006, Article ID 93658, 8 pages
doi:10.1155/2006/93658

*Research Article*

# Optical Coherence Tomography for Tracking Canvas Deformation

**Piotr Targowski,[1] Michalina Góra,[1] Tomasz Bajraszewski,[1] Maciej Szkulmowski,[1] Bogumiła Rouba,[2] Teresa Łękawa-Wysłouch,[2] and Ludmiła Tymińska-Widmer[2]**

[1] *Institute of Physics, Nicolaus Copernicus University, Ul. Grudziadzka 5, 87-100 Toruń, Poland*
[2] *Institute for the Study, Restoration and Conservation of Cultural Heritage, Nicolaus Copernicus University, Ul. Gagarina 9, 87-100 Toruń, Poland*

Received 16 September 2006; Revised 28 November 2006; Accepted 29 November 2006

Recommended by Costas Fotakis

Preliminary results of the application of optical coherence tomography (OCT), in particular in its spectral mode (SOCT), to tracking of deformations in paintings on canvas caused by periodical humidity changes are presented. The setup is able to monitor the position of a chosen point at the surface of a painting with micrometre precision, simultaneously in three dimensions, every 100 seconds. This allows recording of deformations associated with crack formation. For the particular painting model examined, it was shown that the surface moves in-plane towards the corner, and bulges outwards ($Z$-direction) in response to a rise in humidity. Subsequent to the first humidification/drying cycle, translation in the $Z$-direction is decreased, whilst in-plane translations increase somewhat. It was also shown that the response of the painting on canvas begins immediately on changing the relative humidity in the surroundings.



## 1. INTRODUCTION

Differences between environmentally induced dimensional changes in each of the hygroscopic layers composing the multilayer complex of an oil painting on canvas result in deformations, cracks, and detachments between layers, causing severe damage to the structure of the painting. An ongoing research project aims at the gathering of detailed data for a better understanding of the relationships between the painting technique employed, the subsequent history of the painting (age and storage conditions), and its susceptibility to dimensional deformation influenced by fluctuations of relative humidity and temperature, as well as quantifying the range and direction of the changes. The project demands an accurate and convenient method of tracking three-dimensional deformation of the object subjected to environmental stress. The present study was to assess the applicability of optical coherence tomography (OCT) for nondestructive and noncontact monitoring of such deformations in microregions of the surface examined, namely, to estimate the rapidity, range, and direction of dimensional changes in a typical (model) painting on canvas in response to periodical changes of relative humidity.

OCT is a noninvasive technique, well established in medical diagnostics, especially in ophthalmology, where it is routinely used for imaging precise cross-sections of the eye in vivo. This method has also been used for investigating the internal structure of some objects of art, like varnish and glaze layers of paintings on canvas, and also parchment and porcelain objects (see [1] for a brief review). This new application of OCT broadens the spectrum of nonintrusive techniques for measuring deformations and strains occurring in works of art. Among noncontact methods, generally based on optical phenomena, the most popular are double-exposure holography, electronic pattern interferometry and photogrammetry. A review of this subject recently published by Dulieu-Barton et al. [2] contains not only a comprehensive list of references, but also descriptions of all the methods used mainly for examinations of art works made of rigid materials such as plaster, stone, wall paintings, mosaics, ceramics, and panel paintings. A review article by Ambrosini and Paoletti [3] is devoted specifically to methods used for examination of paintings on wooden supports. The

investigation of deformations in flexible materials, for example, paintings on canvas, which are more sensitive to vibrations and strain fluctuations, is significantly more difficult. To the best of our knowledge, the major work in this area is that of Young (e.g., [4–8]), who utilised electronic speckle pattern interferometry (ESPI) combined with tensometry (biaxial tensile tester). These experiments generate maps of in-plane strain distribution over an approximately $30 \times 30$ cm square surface, and are very useful for assessment of conservation methods for local tear mending [6], lining [7], and canvas mounting on stretcher [8]. Varoli-Piazza et al. [9] used image correlation based on stereophotogrammetry to assess the distortions of textile artefacts caused by their display in different orientations. This method—designed for 3D measurement—is less sensitive to vibrations and fluctuations in strain state than ESPI. Among other tools useful for deformation measurements, resistance (ohmic) strain gauges and optical fiber sensors should be mentioned [2]. However, both of these methods require contact (attachment of the sensor to the object), and must be specifically tuned to the properties of the object of interest.

## 2. EXPERIMENT

To track canvas displacement, spectral optical coherence tomography (SOCT)—a new, rapidly growing brand of OCT—was chosen, due to its very high speed of imaging. The instrument consists of a light source of high spatial but low time coherence and a Michelson interferometer. One arm of the interferometer is terminated by the reference mirror, the other contains the collimating optics, which also provide scanning of the probing beam over the surface of the object under investigation. The scattered light is collected back by the same optics and brought to interference with the light from the reference arm. The resulting light is spectrally analysed, and the signal obtained is Fourier transformed.

In this application, SOCT is used as a profilometric tool. The position of the surface of the object investigated is recovered from the dominating frequency of interference fringes superimposed on the light source spectrum. The frequency of these fringes is proportional to the optical path difference in the two arms of the interferometer. The major advantages of using the OCT method for this application lie in *simultaneous* detection of position in 3 dimensions, and in the absence of problems characteristic of methods relying on measurements of phase differences. Phase detection methods usually suffer from some difficulties, in particular phase ambiguity and phase unwrapping, especially in the case of large displacements (the interference fringes are then close, and hard to resolve). In addition, phase detection methods are sensitive to microdisplacements (less than a wavelength) of the investigated object with respect to the measuring head: such a dislocation produces additional, unwanted fringes. Lack of this last effect in OCT simplifies the experimental setup and permits long-lasting examination (up to several days), as well as in situ testing. The major disadvantage is in surface (or in-depth in some modalities) scanning, intrinsic to OCT, which always takes more time than the recording of fringe images, such as in phase interferometry.

The method described here combines profilometry with marker tracking. A substantial advantage of such an approach is its simple and unequivocal displacement recognition, with the disadvantage only of the restriction that displacements are monitored to just one chosen point (or, in the near future, a few points) of the surface. The probing beam is scanned over a rectangular region ($4 \times 4$ mm) of canvas surface to monitor the displacement of the chosen point within this area. Two-directional scanning, which requires collection of $500 \times 500 = 250\,000$ data points, takes only about 12 seconds, which is acceptable for the time-resolved experiments described in this paper. However, it must be admitted that, due to the huge amount of data generated during the scanning, these data must be processed online to reduce the size of information permanently stored. Presently, acquisition and processing takes together about 80 seconds (with a 1.8 GHz AMD Athlon$^{TM}$ 64 processor), which sets a lower limit on the interval between which successive canvas positions can be determined.

The aim of the experiment performed was to track the deformations of a painting on canvas subjected to periodical changes of humidity. These conditions are common in an exhibition area or sacral interior during opening hours, and separated by long intervals with lower relative humidity at night.

Displacements of the canvas surface are a complex result of both slow and fast reactions in separate layers in the multilayer structure of the painting, that also stimulate or restrain changes occurring in other layers. The size layer and linen support react the fastest and the most extensively [10–12]. In paintings made with a technique similar to the sample tested (where the size—applied cold—does not saturate the textile, but fills spaces between treads), dimensional changes in these layers in response to relative humidity rises are usually opposing. Contraction of the canvas in the warp and weft directions resulting from an increase in the crimping of the swelling threads is decreased to some extent by wedges of gelatine glue separating threads and expanding due to their hygroscopic nature. Contraction of the size during drying stresses the whole structure of the painting. The comparatively stiff ground layer and oil paint film respond to both increases and decreases in humidity at a smaller rate and with longer delay. They resist displacements of their support until the moment at which the stress exceeds their cohesion, at which point they crack.

The wooden stretcher also influences the behaviour of the whole painting. Its resistance can prevent contraction of the painting in response to a rise in humidity and thus increase the stress in the structure. The later delayed expansion of the wood can even create additional tension.

## 3. MATERIALS AND METHODS

### 3.1. Sample

The painting tested in the present study was chosen from a series of 80 samples prepared with the intention of producing

models that would best represent properties of real paintings.

Modern commercial linen canvas of medium thickness and close weave (15 threads of warp and 13 threads of weft per cm$^2$, and filling factors, defined in [10, 11] as the percentage projected surface area occupied by threads, calculated as the product of the number density of threads and their average width—$Z_{\text{weft}} = 68\%$, $Z_{\text{warp}} = 70\%$, $Z_{\text{total}} = 90\%$) was used. This canvas was prepared by stretching over a keyed pinewood stretcher (height 30 cm, width 40 cm) with weft in the vertical direction. Staples were used to secure the canvas at hand tension. A cold 5% gelatine size was applied with a spatula and followed by two layers of emulsive gesso serving as priming. Three layers of casein tempera and one of alizarin oil glaze were used to imitate an old paint layer. The sample was tested after six months of seasoning in the ambient conditions of a conservation studio.

### 3.2. Experimental setup

To create periodical changes in the environment of the sample, an airtight compartment was designed (Figure 1(a)). Its front wall was made of 2 mm glass to allow optical scanning. The humidity increment is induced by trickling water down over a piece of cotton fabric which is hung 15 cm behind the back of the canvas support. The consecutive decrease of humidity (to ambient level) is achieved by ventilation of the compartment. During all experiments, the temperature and relative humidity inside the chamber were monitored with a HygroClip *S* sensor from Rotronic (Switzerland). To simulate the effect of variable environmental conditions on a painting, the model was subjected to two cycles of rapid humidification (see Figure 4, upper panel in results section), lasting for 1.5 hours (up to 90% RH) in every 24 hours, over four days. The cycles were separated by a 1.5-hour period of drying to ambient conditions. The temperature remained fairly constant.

To monitor the position of a chosen point on the canvas, a small reference marker dot ($\sim 0.4$ mm in diameter) of good reflective paint is placed on the paint layer. This marker was located in the bottom right corner, 5 cm from both edges of the canvas (Figure 1(b)), just at the boundary of the area of the canvas covered by the wooden stretcher bar. This position was chosen due to the moderate displacement of this area as compared with that of the central area of the canvas noted previously in [13, 14], and confirmed here in preliminary tests. The positive $X'$-coordinate axis points towards the vertical canvas edge, parallel to the warp direction, the $Y'$-axis away from the lower horizontal edge, parallel to the weft direction. The $Z'$-axis points out of the canvas.

The details of the SOCT instrument used in this study are described elsewhere in this volume [15]. However, it is worthwhile to repeat here that the instrument utilises a superluminescent diode emitting light of central wavelength 835 nm and spectral width (FWHM) 50 nm. The axial (in-depth) resolution obtained was 8 $\mu$m (in air). The light, of $\sim 200\,\mu$W intensity, is focused at the object surface to a spot of $\sim 15\,\mu$m in diameter. It should be noted that the resolutions defined above relate to ordinary cross-sectional imaging. However, in the case of this study, information on displacement is drawn from repeated analysis of the same object, that is, the reference marker. As a result, the real resolution of the displacement measurement depends also on details of the procedures used for data collection and analysis, and must in practice be determined experimentally. For present purposes, this was accomplished by consecutive measurements of the position of the test object, held steady in the $X, Y$ plane, and precisely translated in the $Z$-direction. Repeatability of the $X, Y$ determination may be considered as a measure of the lateral resolution, and similarly the resolution of the $Z$-coordinate as a measure of axial resolution. It is not surprising that the lateral and $Z$-coordinate resolutions (8 $\mu$m and 2 $\mu$m, resp.) obtained from such a procedure are both smaller than the expected (theoretical) ones cited above, since here it is the same object that is being tracked, and relative displacements that are being recovered. In addition to resolution, a second factor decisive for the application of the method described is the range of translation which it is possible to monitor. For in-plane translation, the latter is limited by the dimensions of the scanned area (here, $4 \times 4$ mm), and thus may be estimated to be 2 mm in any in-plane direction. For axial translations, the range is equivalent to the depth of cross-sectional imaging, and is limited by optical properties of the OCT instrument [1]. For the system employed here, the axial range is thus about 1 mm in both (inward and outward) directions. These resolutions and ranges determine the available range over which the effects examined may be investigated, and limit the variety of environment conditions which may be studied.

### 3.3. Data analysis

Data collection and analysis were performed online in the following 4 steps.

*Step 1* (data collection). Volume data for analysis were collected by scanning over a square area $4 \times 4$ mm, usually composed of $500 \times 500$ pixels. By integrating the OCT signal over the whole depth of scanning, a 2D image of the sample surface is prepared (Figure 2(a)) and used for marker recognition (Step 2). Depth data are used for $Z$-coordinate recovery (Step 3).

*Step 2* (marker recognition and tracking). An image of the marker is stored during the first measurement. In consecutive following measurements, the position of the marker is automatically recovered by seeking the maximum of the 2D correlation function between the new image of the canvas ($I(x, y)$) and the stored image of the marker ($P(x, y)$):

$$C(x,y) = I(x,y) \otimes P(x,y) = \iint I(x,y) \otimes P(x+t, y+s)\,dt\,ds,$$
$$(X,Y) : C(x,y) = \text{Max}, \tag{1}$$

where $I(x, y)$ denotes the newly registered image of the canvas, $P(x, y)$ is the stored image of the marker, and $C$ is the

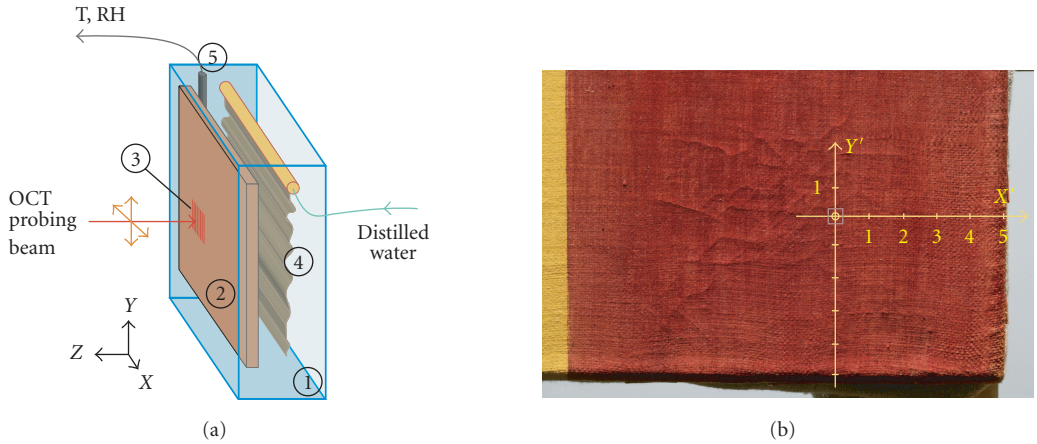


Figure 1: (a) The climate control sample compartment used in the study: (1) airtight chamber with a glass front wall, (2) sample: a painting on canvas on a stretcher, (3) scanned area of the paint layer, (4) cotton fabric used to increase humidity, (5) temperature and relative humidity sensor. (b) Position of the marker (small circle) and the scanned area (square). Axes indicate the orientation of the sample coordinate system.

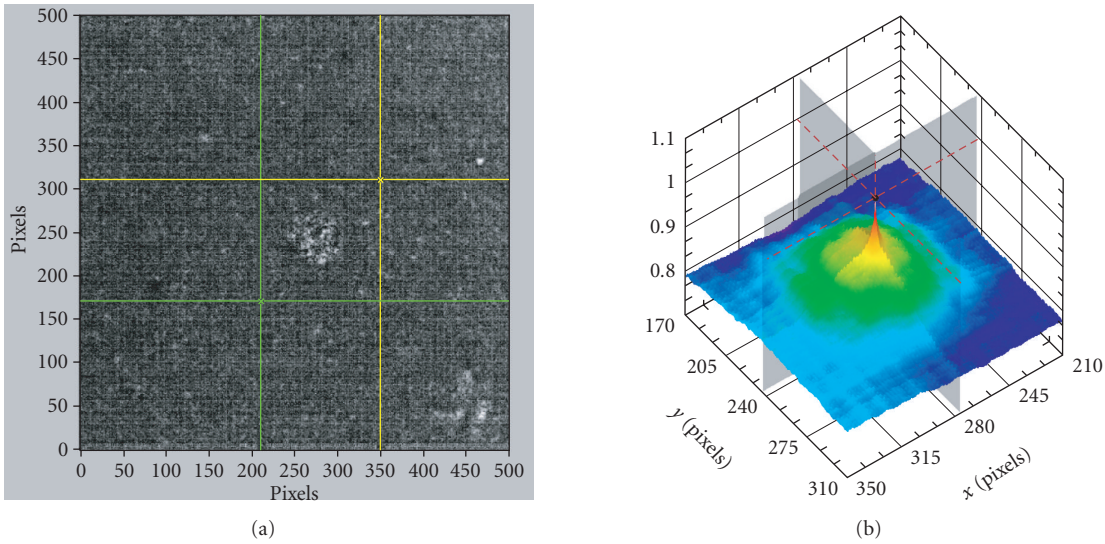


Figure 2: (a) A 2D image of the scanned area (Figure 1(a)-3); the marker is visible as a lighter spot in the centre, within the cursor lines. (b) The correlation function $C(x, y)$: the maximum of this function gives the position of the marker.

correlation function (Figure 2(b)). $X, Y$ are the recovered coordinates of the marker in the laboratory coordinate system.

*Step 3* ($Z$-coordinate determination). The $Z$-coordinate of the marker is recovered from OCT A-scans. The A-scans from the area centred on the position of the image marker $(X, Y)$ are averaged, and the $Z$-coordinate is recovered from this averaged signal. A position index of the maximum of this averaged signal is recovered. The relative $Z$-coordinate is calculated by multiplying the position index by an FFT scale coefficient (4 $\mu$m/FFT bin in the system described). This coefficient depends on the design of the spectrometer and can be obtained by calibration.

The resolution of the $Z$-coordinate determination depends on the algorithm used in the peak detection subroutine. The subroutine uses a least squares quadratic fit to find the peaks; thus the index value is fractional rather than integer.

*Step 4* (marker coordinates transformation). The marker coordinates $(X, Y, Z)$ obtained must be transformed to the sample coordinate system $(X', Y', Z')$—Figure 3(a). To define these new coordinates, it is assumed that the sample $Z'$-axis is normal to the sample surface and that the sample $X'$-axis remains in the horizontal $X, Z$ plane.

This new system is attached to a plane obtained by fitting to the surface profile recovered from the OCT data—Figure 3(b). The procedure of determining the coordinate transformation is performed once for the experiment—it is

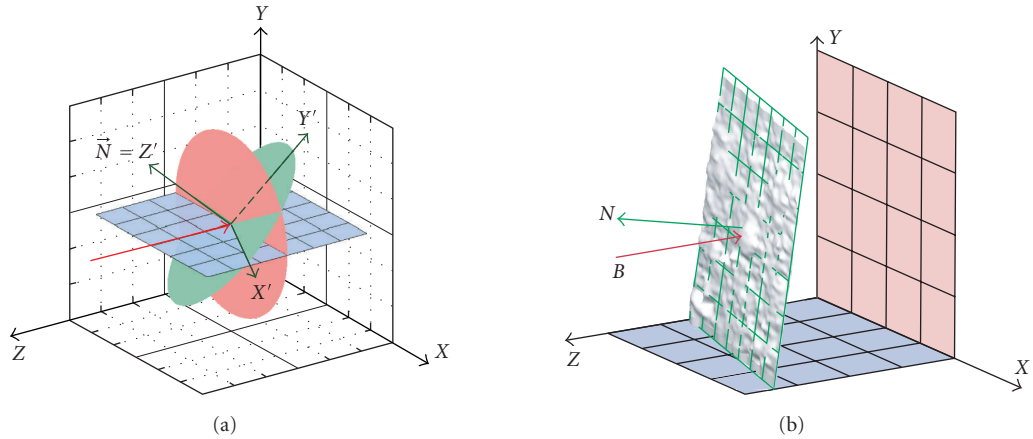


FIGURE 3: (a) mutual orientation of the two coordinate systems. The red plane denotes the $(X, Y)$ surface in the laboratory system, the green one denotes the sample surface. Vector $\vec{N}$ is normal to the sample surface. (b) The sample plane (green mesh) is obtained by fitting to the surface profile. The red arrow (parallel to the $Z$-axis) denotes the OCT probing beam.

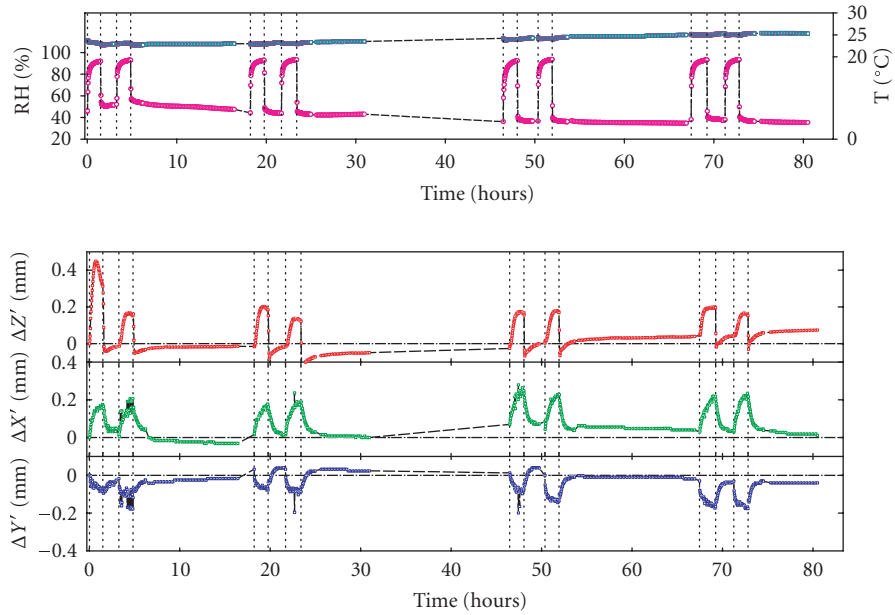


FIGURE 4: Displacements of the position of the marker at the surface of the sample in response to periodical changes in relative humidity (RH, the upper panel).

assumed that the stretcher remains in a constant position thereafter. The details are given in the appendix.

## 4. RESULTS AND DISCUSSION

The experiment set-up was to monitor the behaviour of painting on canvas subjected to simulated periodical changes of humidity in its surroundings. Within four days, slight but clearly visible cracks had appeared, running across the paint and ground layers (Figure 1(b)). On the microscale, small movements (up to 0.4 mm) of the marker on the surface of the paint layer were observed (Figure 4 and supplementary file). Preliminary tests showed that the choice of the point to be tracked by OCT on the surface of the painting is crucial, as displacements recorded during climatic change are different in the centre of the painting than at the edges, especially those in the $Z$-direction. For the present tests, a point in a region of the canvas exhibiting moderate deformation was chosen.

Changes in $\Delta X'$, $\Delta Y'$, and $\Delta Z'$ of the marker with respect to its initial position were observed immediately after

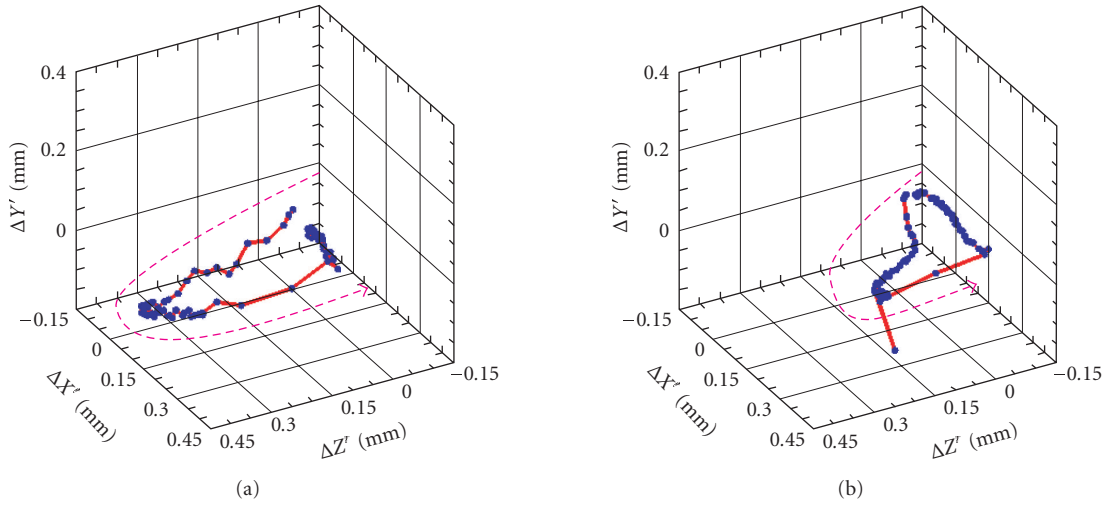


Figure 5: Traces of marker displacements during the first (a) and fourth (b) humidification cycles. Notice the spike evident in panel (b).

every variation in climatic condition. The translation in the $X'$-$Y'$ plane caused by rise of humidity was directed towards the (near) corner of the painting—see also the AVI movie attached. This displacement was accompanied by simultaneous outward movement (towards the OCT instrument, positive $Z'$-direction). Around 85% RH, this reaction is reversed: the marker was moving back slightly (negative $Z'$).

Rapid drying out of the test chamber caused an immediate and strong reaction of the painting in the negative $Z'$-direction: the marker was moving back behind the initial (before humidification) plane, and then relaxing to the initial position during drying in ambient conditions. In contrast with in-plane translations, the movement in the $Z'$-directions does not simply follow the humidity—the direction alternates during a monotonic change in humidity conditions.

In the $X'$-$Y'$ plane, the general form and features of the changes ($\Delta X'$ and $\Delta Y'$ curves) are the similar, although larger displacements were registered in the $X'$-direction parallel to the warp and the long stretcher bar. It is difficult to judge if disproportion in reaction along the $X'$- and $Y'$-axes results from the difference in the dimensions of the sample in the two directions, or from the dominance of the overall anisotropic reaction of the canvas itself: for contemporary linen canvases, it is quite common that the warp is less stiff and more susceptible than the weft to dimensional deformation influenced by fluctuations of relative humidity [16–18]. It is important to point out the somewhat irregular character of the $\Delta X'$ and $\Delta Y'$ curves. We believed that the spikes, visible in the $\Delta X'$ and $\Delta Y'$ curves, but not in the $\Delta Z'$ curves, are due to a sudden relaxation of tension in the structure—possibly due to the formation of cracks in the paint layer (such cracks were observed after the experiment), or to rapid movements of the weave or of separate threads in the canvas.

The first day of humidification cycling exhibits somewhat different behaviour, both qualitatively and quantitatively. The effects of the first climate shock are very different to those of the consecutive ones. This first response in the direction perpendicular to the canvas surface ($Z'$) is significantly stronger than that found in the following ones. This is not the case for in-plane displacements, in which the $Y'$ displacement was even somewhat less than in consecutive cycles. The first humidification cycle in the experiment described was also the first major environmental stress applied to the picture, which had previously been stored in ambient conditions. The painting probably settled down on the stretcher during this first cycle of rapid humidification. During the second humidification cycle on the first day, several spikes were observed in the curves representing changes in the $X'$-$Y'$ plane. Probably, this second climatic shock and rapid rise of tension in the multilayer composite (caused by shrinkage of canvas restrained by the stretcher, and/or expansion of the size and priming layer) resulted in crack formation in the stiffest layers.

In the curves representing further consecutive cycles, spikes only show up around the maximal values of displacement, and they are more prominent in the $\Delta Y'$ curves representing changes in the sample vertical (weft). It is significant that spikes occur during humidification but not during drying.

Comparing the three-dimensional marker displacement traces during the first (Figure 5(a)) and subsequent cycles (the fourth, e.g., Figure 5(b)), it is again evident that, although in all cycles there is hysteresis in the sample deformation (indicating some persistence in deformation), the response to the first climate shock is very different to that of the consecutive ones.

The complicated changes described above reflect the complexity of reactions influencing the behaviour of the whole of the multilayer structure of the painting on canvas. Displacement of the picture in $Z'$-direction could be caused directly or secondarily: it could result from the movement of

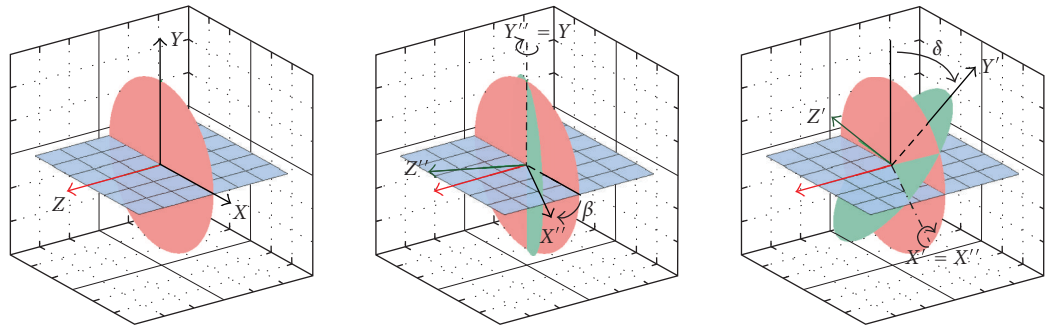


FIGURE 6: (a) The laboratory coordinate system, (b) rotation about $Y''$ through angle $\beta$, (c) rotation about $X'$ through angle $\delta$.

the whole structure due to a change of tension in the painting on the stretcher, bulking of the face caused by uneven shrinkage or expansion of various layers in the composite, and/or change in the thickness of the structure resulting from swelling of hygroscopic layers, as well as out-of-plane distortions in particular sections of the cracked gesso and paint layer.

## 5. CONCLUSIONS

The present test studies confirmed that OCT is capable of continuously tracking deformation of paintings, with micrometer resolution, simultaneously in three dimensions. Registration of the deformation is automatic, and was made at a high rate (every 100 seconds) over a period of four days. As demonstrated, this permits monitoring of the course of long-term reactions of the painting, including crack formation, to rapid climate changes. The method allows investigation of the relationship between in-and-out-of-plane displacements, and recording of rapidly changing deformations. Although the resolution of the method is somehow lower than that of other available optical techniques, it is combined with a high range of accessible displacements. This allows the tracking of reactions to large changes in environment conditions, but has enough precision for tracking responses to moderate humidity jumps also. Modification of the sample compartment to allow more precise control of humidity conditions is under way.

With regard to the model painting examined, it was shown that, in response to a rise in humidity, the surface moves towards the nearest corner in plane, and bulges outwards. After the first humidification/drying cycle, translations in the $Z'$-direction are smaller, whilst in-plane translations increase somewhat. It was also shown that the response of the painting on canvas occurs immediately on changing the relative humidity in the surroundings.

To improve our understanding of processes taking place in the structure of the painting in response to rapid climate changes, and to interpret the role of particular components in the behaviour of the overall structure, model paintings prepared using different techniques, and samples at different stages of preparation will be examined in further tests. These experiments will be carried out with pictures mounted on wooden stretchers, as well as on stretchers inert to humidity. Simultaneously, the stress in the painting-stretcher system will be monitored with other methods.

## APPENDIX

Before applying any environmental stress to the sample, its initial position must be recovered. To do so, a profile of the canvas surface is first determined from the OCT data, essentially as described elsewhere [19], then the plane is fitted to this profile. If the equation of this plane has the canonical form: $A \cdot x + B \cdot y + C \cdot z + D = 0$, then the coordinates of a vector $\vec{N}$normal to fitted plane are given by

$$N_X = \frac{A}{\sqrt{A^2 + B^2 + C^2}}, \qquad N_Y = \frac{B}{\sqrt{A^2 + B^2 + C^2}}, \qquad N_Z = \frac{C}{\sqrt{A^2 + B^2 + C^2}}. \tag{A.1}$$

The coordinates of this vector contain all available information about the position of the $X'$-$Y'$ plane with respect to which the sample surface is described. To make the transformation between coordinates unambiguous, an additional assumption is necessary: the $X$-axis remains in the horizontal plane (marked blue in Figure 6). To transform the laboratory coordinates ($X, Y, Z$ in Figure 6(a)) into the sample coordinates ($X', Y', Z'$ in Figure 6(c)), the following two rotations are necessary.

(i) The ($X''$, $Y''$, $Z''$) axes result from rotation of the ($X$, $Y$, $Z$) axes about $Y$ through an angle $\beta$, clockwise relative to the $X$-$Z$ plane (Figure 6(b)). The $X''$-axis remains in the horizontal plane and coincides with the sample plane.

(ii) The ($X'$, $Y'$, $Z'$) axes result from rotation of the ($X''$, $Y''$, $Z''$) axes about $X''$ through an angle $\delta$ clockwise relative to the $Y''$-$Z''$ plane (Figure 6(c)). The $X''$ and $X'$ axes coincide.

The matrices describing these rotations may be multiplied to give the overall rotational matrix:

$$\begin{bmatrix} 1 & 0 & 0 \\ 0 & \cos(\delta) & -\sin(\delta) \\ 0 & \sin(\delta) & \cos(\delta) \end{bmatrix} \cdot \begin{bmatrix} \cos(\beta) & 0 & \sin(\beta) \\ 0 & 1 & 0 \\ -\sin(\beta) & 0 & \cos(\beta) \end{bmatrix} = \begin{bmatrix} \cos(\beta) & 0 & \sin(\beta) \\ \sin(\delta)\cdot\sin(\beta) & \cos(\delta) & -\sin(\delta)\cdot\cos(\beta) \\ -\cos(\delta)\cdot\sin(\beta) & \sin(\delta) & \cos(\delta)\cdot\cos(\beta) \end{bmatrix}. \tag{A.2}$$

The vector $\vec{N}$ normal to the sample surface has coordinates $(N_X, N_Y, N_Z)$ in the laboratory system, and coordinates (0, 0, 1) in the sample system. Then angles $\beta$ and $\delta$ may be obtained from

$$\begin{bmatrix} \cos(\beta) & 0 & \sin(\beta) \\ \sin(\delta)\cdot\sin(\beta) & \cos(\delta) & -\sin(\delta)\cdot\cos(\beta) \\ -\cos(\delta)\cdot\sin(\beta) & \sin(\delta) & \cos(\delta)\cdot\cos(\beta) \end{bmatrix} \cdot \begin{bmatrix} N_X \\ N_Y \\ N_Z \end{bmatrix} = \begin{bmatrix} 0 \\ 0 \\ 1 \end{bmatrix} \tag{A.3}$$

giving

$$\tan(\beta) = -\frac{N_X}{N_Z} = -\frac{A}{C}, \qquad \sin(\delta) = N_Y = \frac{B}{\sqrt{A^2 + B^2 + C^2}}. \tag{A.4}$$

Since both angles are small, formulas (A.4) are unambiguous. This procedure is performed once, at the beginning of the experiment, and matrix (A.2) is then used to transform all data retrieved.

## ACKNOWLEDGMENTS

This work was supported by Polish Ministry of Science Grant no. 2 H01E 025 25. Authors wish to thank Professor Tadeusz Marszalek and Dr. Robert Dale for their very valuable discussions. The third author gratefully acknowledges the support of a Foundation for Polish Science Scholarship for Young Researchers.

## REFERENCES

[1] P. Targowski, M. Góra, and M. Wojtkowski, "Optical coherence tomography for artwork diagnostics," *Laser Chemistry*, vol. 2006, Article ID 35373, 2006.

[2] J. M. Dulieu-Barton, L. Dokos, D. Eastop, F. Lennard, A. R. Chambers, and M. Sahin, "Deformation and strain measurement techniques for the inspection of damage in works of art," *Reviews in Conservation*, vol. 6, pp. 63–73, 2005.

[3] D. Ambrosini and D. Paoletti, "Holographic and speckle methods for the analysis of panel paintings. Developments since the early 1970s," *Reviews in Conservation*, vol. 5, pp. 38–48, 2004.

[4] C. Young, "Quantitative measurement of in-plane strain of canvas paintings using ESPI," in *Applied Optics Division*, pp. 79–84, Institute of Physics, IOP, Brighton, UK, 1998.

[5] C. Young, "Measurement of the biaxial properties of nineteenth century canvas primings using electronic speckle pattern interferometry," *Optics and Lasers in Engineering*, vol. 31, no. 2, pp. 163–170, 1999.

[6] C. Young, "The mechanical requirements of tear mends," in *Alternatives to lining, BAPCR & UCIK Conference*, pp. 55–58, September 2003.

[7] C. Young, R. Hibberd, and P. Ackroyd, "An investigation into the adhesive bond and transfer of tension in lined canvas paintings," in *Proceedings of the 13th Triennial Meeting of the ICOM Committee for Conservation (ICOM-CC '02)*, pp. 370–378, Rio de Janeiro, Brazil, September 2002.

[8] C. Young and R. Hibberd, "The role of canvas attachments in the strain distribution and degradation of easel paintings," in *Tradition and Innovation: Advances in Conservation, Contributions to the IIC Melbourne Congress*, pp. 212–220, London, UK, October 2000.

[9] R. Varoli-Piazza, R. Rosicarello, M. Giorgi, and J. Bridgland, "The use of photogrammetry in determining the correct method of displaying a textile artefact: the cowl of St. Francis of Assisi," in *Proceedings of the 11th Triennial Meeting of the ICOM Committee for Conservation (ICOM-CC '96)*, pp. 726–731, Edinburgh, Scotland, September 1996.

[10] B. Rouba, "Płótna jako podobrazia malarskie (canvases as painting supports)," *Ochrona Zabytków*, vol. 38, pp. 227–244, 1985.

[11] B. Rouba, "Die Leinwandstrukturanalyse und ihre Anwendung für Gemäldekonservierung," *Restauratorenblätter*, vol. 13, pp. 79–90, 1992.

[12] B. Rouba, *Podobrazia płócienne w procesie konserwacji (Canvas Painting Supports in the Process of Conservation)*, Wydawnictwo UMK, Toruń, Poland, 2000.

[13] G. A. Berger and W. H. Russell, *Conservation of Paintings*, Archetype, London, UK, 2000.

[14] B. Rouba, "Rückseitenschutz für Leinwandbilder - eine Methode von Eigenschafteenuntersuchungen," in *Proceedings of the 4th International Conference of Non-Destructive Testing of Works of Art*, pp. 657–669, Berlin, Germany, October 1994.

[15] M. Góra, P. Targowski, A. Rycyk, and J. Marczak, "Varnish ablation control by optical coherence tomography," *Laser Chemistry*, vol. 2006, Article ID 10647, 2006.

[16] C. R. T. Young and R. D. Hibberd, "Biaxial tensile testing of paintings on canvas," *Studies in Conservation*, vol. 44, no. 2, pp. 129–141, 1999.

[17] A. Guzowska, "Przygotowanie płócien dublażowych (preparation of lining supports)," M.A. thesis, Department of Conservation of Paintings and Polychrome Sculpture, Nicolaus Copernicus University, Toruń, Poland, 1996, B. Rouba, Advisor.

[18] L. Tymińska, "Uzupełnianie ubytków w podobraziach płóciennych—próba opracowania nowej metody z wykorzystaniem płynnej masy włóknistej (Filling voids in canvas painting supports—experiment on developing a new method with the use of liquid fibrous pulp)," M.A. thesis, Department of Conservation of Paintings and Polychrome Sculpture, Nicolaus Copernicus University, Toruń, Poland, 2002, M. Roznerska and B. Rouba, Advisors.

[19] P. Targowski, T. Bajraszewski, I. Gorczyńska, et al., "Spectral optical coherence tomography for nondestructive examinations," submitted to *Optica Applicata*.